Met Office

Development of Radiation Schemes for the Extended Unified Model

David Jackson, Emily Down and James Manners

Introduction

The Met Office aims to extend its Unified Model (UM) for weather and climate into a whole-atmosphere model to simulate the atmosphere from the surface to the thermosphere above altitudes of 100km. A key part of this work is the extension of the UM radiation scheme to cover non local thermodynamic equilibrium (LTE) processes, and the Far Ultraviolet (FUV) and Extreme Ultraviolet (EUV) part of the spectrum. Progress in these areas is described here.

This work is an important part of the EU Horizon 2020 project: SWAMI (Space Weather Atmosphere Model and Indices).

MLT radiation requirements

The requirements for radiative transfer (RT) in the mesosphere and lower thermosphere (MLT) differ to those in the lower atmosphere.

Non LTE: The existing UM radiation scheme assumes prime radiative heating and cooling mechanisms are close to LTE. However, above around 70 km this ceases to be a good approximation and representation of non-LTE radiative heating is required. Figure 1 shows that total non-LTE solar heating starts to deviate from the LTE values at around 65 km. At 95 km the difference in heating rates exceeds 20 K day^{-1}. Similarly infrared cooling rates start to diverge around 85 km. We address this by implementing the non-LTE radiative scheme developed by [1]. It represents both non-LTE infrared cooling (15 µm CO_2 & 9.6 µm O_3 bands) and non-LTE heating (1.05 - 4.3 µm CO_2 and 200-310nm O_3 bands).

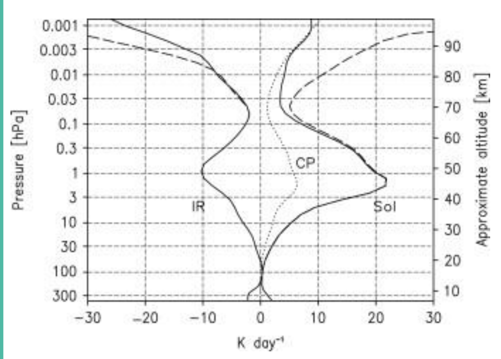

Figure 1: Radiative energy terms for the tropical atmosphere, with an overhead Sun. Solid and dashed lines show values for NLTE and LTE respectively. From [1]

FUV and EUV: The SW part of the UM radiation code only includes wavelengths of greater than 200 nm. Figure 2 shows no solar irradiance with wavelengths less than ~ 200 nm penetrates below the mesopause. However, for modelling the 85-170 km region, the UM also needs to represent RT from the FUV (122-200 nm) and EUV (10-121 nm) parts of the spectrum. In addition to extending the calculation of radiative heating rates, this change will also provide actinic flux required to calculate the photolysis rates for key exothermic chemical reactions in the MLT.

Figure 2: Solar irradiance atmospheric penetration depth, unitary optical depth, for photons from hard X-rays to 300 nm. From [2].

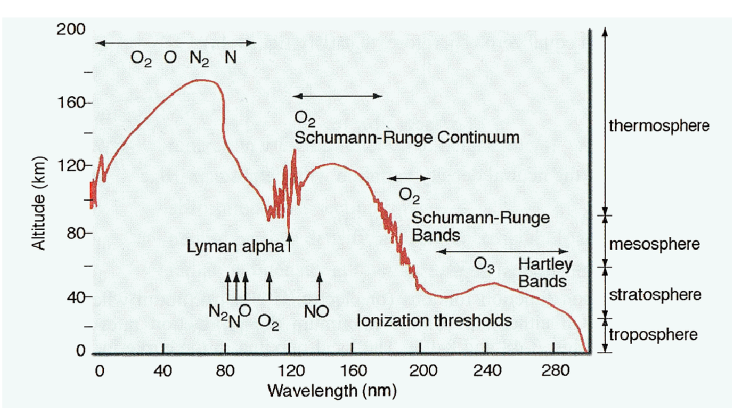

Chemical heating & MLT Heat Budget

Figure 3 shows MLT heating rates from a WACCM simulation. Heating from the EUV part of the spectrum (short dashed line) becomes increasingly important from around 100 km to 130 km. However, the largest contribution to heating comes from chemical heating (solid line). These two contributions are required in order to simulate the large increase in temperature with altitude observed above around 90 km. In separate work, the relevant chemical reactions are being added to the UM. These reactions require photolysis rates from the FUV / EUV extension to the UM radiation scheme.

Figure 3: WACCM global mean heating rates (K day^{-1}), for July at solar minimum. CHEM: chemical heating, QUV and QEUV: thermalized radiation for UV and EUV bands, NIR CO2: heating by CO2 absorption in the near-infrared, AURORA: thermalized energy from particle precipitation,JOULE: joule heating. (from Marsh et al, 2007).

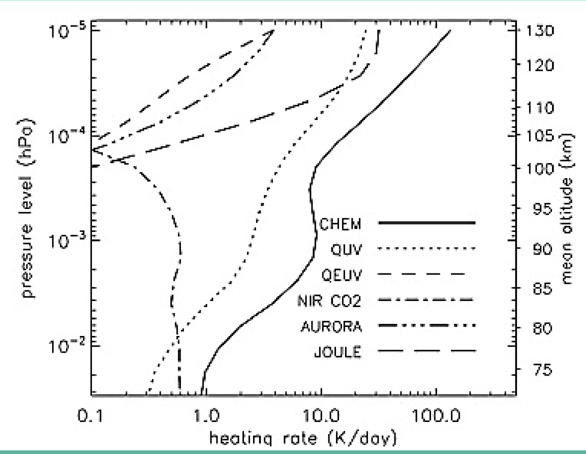

Progress with FUV / EUV Radiation

A flexible new photolysis scheme has been implemented in the UM RT code. Spectral absorption lines can vary dramatically over very small wavelength intervals. The **correlated-k method** bins up wavelengths with similar absorption coefficients, so RT calculations need then only be done for each bin. The novel technique here is to retain the information on the wavelengths that each k-term represents. Once the RT calculations have been done, the fluxes for each k-term are mapped back to these wavelengths. The high resolution fluxes are then convolved with the solar spectrum, absorption cross-sections and quantum yields to derive accurate photolysis rates. Spectra can be diagnosed at high-resolution, effectively providing line-by-line resolution for the cost of a broad-band calculation (e.g. Figure 4).

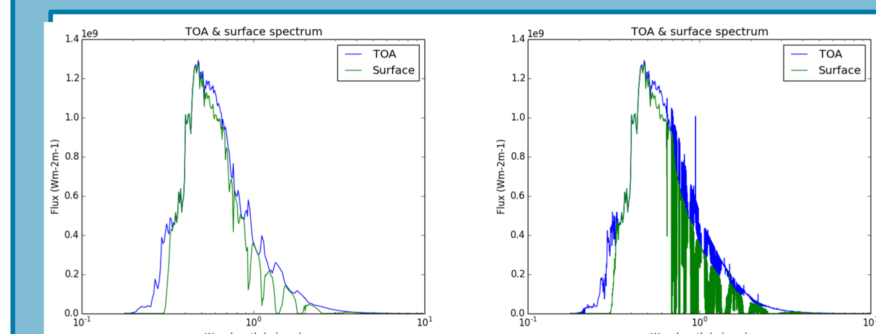

Figure 4: Example net SW fluxes over the standard 260 bands (left) and over 98000 channels (right) using the mapping technique developed here.

The **photolysis or photoionisation rate** for a given molecule is calculated using actinic flux, absorption cross-section and quantum yield. The quantum yield is parametrised at arbitrary resolution and is read in as part of a configuration file, to which any photolysis reaction can be simply added, thus ensuring flexibility. Summation over channels is done by weighting each channel by the incoming solar spectrum. **The radiative heating rate** is determined using the flux divergence across a layer. Where photolysis occurs some of the absorbed flux is used for dissociation or ionisation. This energy is therefore not (immediately) available to increase the kinetic energy of the gas and should instead be handled by the chemistry scheme. We calculate the proportion of the flux used for photolysis by finding the fraction of energy in each photolysing photon that is needed to break the bonds and produce the given photolysis products.

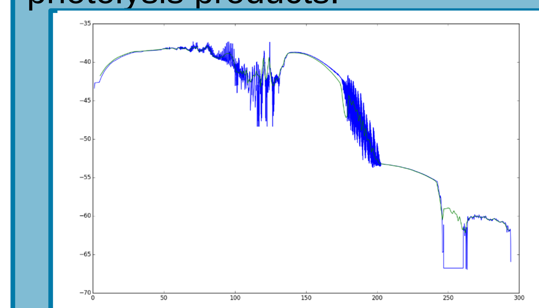

Figure 5: O_2 absorption cross-sections in FUV / EUV. x-axis shows wavelength in nm, y-axis shows log (absorpn strength) in cm2/mol. The blue line shows the high-res data used here. The green line is an earlier dataset meaned over 1nm bins.

<u>**Narrow-band configuration for the FUV and EUV:**</u> an initial configuration covering 0.5 – 320.5nm has been developed with the aim of producing an accurate reference configuration to benchmark an eventual fast broad-band configuration. Here, we use the following gas absorbers: H_2O, CO_2, O_3, N_2O, CO, CH_4, O_2, NO, NO_2, N_2, H_2. Gas absorption coefficients are derived from recommendations from JPL Currently, only O_2 absorption is used in the highest resolution available (Figure 5). The other gases currently use coefficients meaned in 1nm bands.

O_2 is currently treated as the major gas where cross-sections are available. With the k-term mapping technique applied this results in 8175 channels over the 320 bands with the channels concentrated in the complex parts of the spectrum such as the Schumann-Runge bands at 175-195nm and wavelengths shortward of 130nm associated with the Rydberg states of oxygen. Photolysis pathways have been included for:

1) O_2 + hv -> O(3P) + O(3P) ; threshold wavelength = 242.3nm
2) O_2 + hv -> O(3P) + O(1D) ; 175nm

Along with photoionisation pathways:

3) O_2 + hv -> O_2+ ; 102.78nm
4) O_2 + hv -> O+ + O ; 66.2nm

This configuration has been run using a test atmospheric profile with gas mixing ratios up to ~120km for "tropical" conditions. The resulting actinic flux is shown in Figure 6, which shows its reduction as we go further down into the atmosphere.

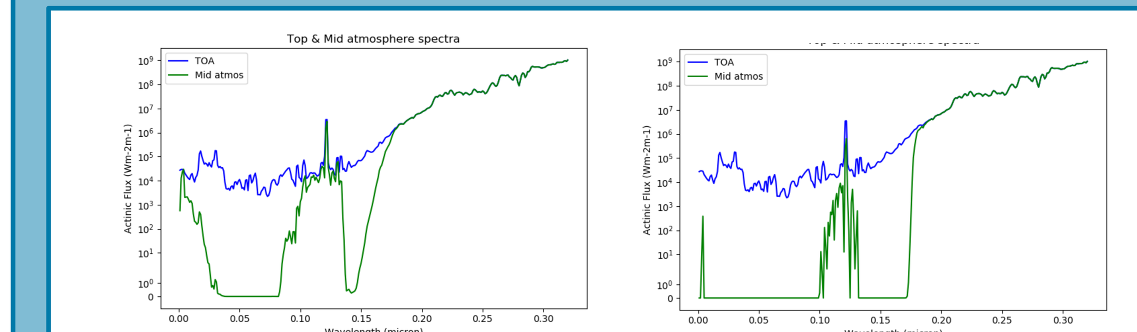

Figure 6: Left: actinic flux at top of atmosphere (blue) and at 110 km (green). Right: like left hand panel, but with actinic flux at 90 km (green).

Photolysis rates for the 4 included pathways are shown in Figure 7. Reaction 1) occurs all the way down through the mesosphere whilst the other pathways only really happen in the thermosphere (not shown). There is a window in the O_2 absorption around the solar Lyman-alpha line (0.1216 µm), so this part of the spectrum is significant, particularly for reaction 2).

Non-LTE results

The Fomichev code was implemented in the UM. The radiative heating is calculated twice, once with the existing LTE scheme and once with the Fomichev scheme, and the heating rates blended at 0.1 hPa (~65km), where non-LTE processes begin to be important. Figure 8 shows the SW heating rates from selected UM output. The largest heating rates (blue) correspond to Sun overhead conditions, and it is clear that, similar to Figure 1, the excessive LTE SW heating has been removed and replaced by a smaller non-LTE heating rate. The other lines in Figure 4 show SW heating for locations with lower solar insolation and the heating rates are accordingly smaller. Non LTE and LTE LW heating rates (not shown) also show a similar pattern to that seen in Figure 1.

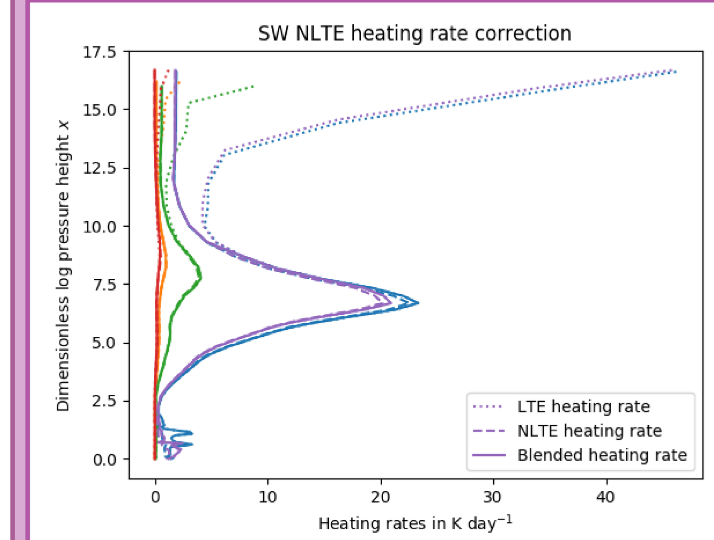

Figure 8: SW LTE (dotted), non-LTE (dashed) and blended (solid) heating rates (K day^{-1})for a selection of UM points. X = ln (1000 / p) is a dimensionless parameter used in the non-LTE scheme formulation. As a guide, x = 9.2 corresponds to p = 0.1 hPa, and x = 12.0 corresponds to p = 0.006 hPa (or around 85 km)

When the non-LTE scheme is included in the UM the zonal wind simulation is close to climatology [see Dan Griffin's poster for more details].

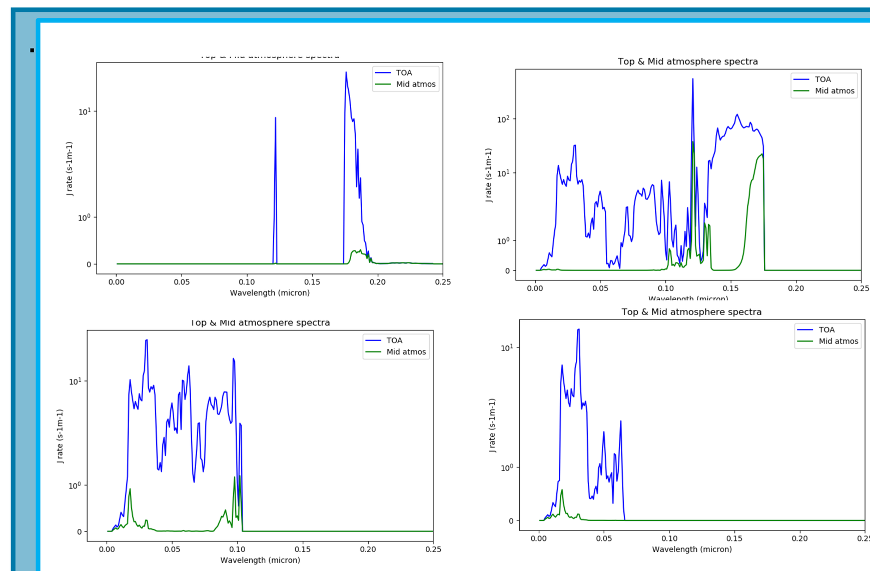

Figure 7: Spectral breakdown of photolysis / photoionisation rates ($m^{-1}s^{-1}$) for reactions 1-4 (top left, top right, bottom left, bottom right, respectively) at ~80 km, ~110 km, ~118 km and ~118 km, respectively (green) and at the top of the atmosphere (blue).

Summary

The non-LTE scheme has been successfully added to the UM, and considerable developments have been made to include FUV / EUV RT calculations and associated calculations of photolysis rates to ensure that the MLT heat budget in the UM can be more accurately calculated. These are key steps in the development of an accurate UM version that extends up to around 150 – 170 km altitude, which is a key objective of the SWAMI project

Met Office FitzRoy Road, Exeter, Devon, EX1 3PB United Kingdom
Tel: +44 1392 8845300 Fax: +44 1392 885681
Email: david.jackson@metoffice.gov.uk

References and Acknowledgments

[1] Fomichev, V. I. (2009). The radiative energy budget of the middle atmosphere and its parametrization in general circulation models, J. Atmos. Terr. Phys., 71, 1577-1585
[2] Chamberlain, J. W. (1978). Theory of Planetary Atmospheres, An Introduction to Their Physics and Chemistry, Int. Geophys.Ser., vol. 22, p.18, Academic, Orlando, Fla., 1978
[3] Marsh, D. R., et al. (2007). Modeling the whole atmosphere response to solar cycle changes in radiative and geomagnetic forcing. J. Geophys. Res., 112, D23306, doi:10.1029/2006JD008306

This project has received funding from the European Union's Horizon 2020 research and innovation programme under grant agreement No 776287.